JOURNAL OF GEOPHYSICAL RESEARCH, VOL. 112, B04405, doi:10.1029/2006JB004596, 2007

Earthquake swarms driven by aseismic creep in the Salton Trough, California

R. B. Lohman[1] and J. J. McGuire[2]

Received 21 June 2006; revised 18 October 2006; accepted 28 November 2006; published 10 April 2007.

[1] In late August 2005, a swarm of more than a thousand earthquakes between magnitudes 1 and 5.1 occurred at the Obsidian Buttes, near the southern San Andreas Fault. This swarm provides the best opportunity to date to assess the mechanisms driving seismic swarms along transform plate boundaries. The recorded seismicity can only explain 20% of the geodetically observed deformation, implying that shallow, aseismic fault slip was the primary process driving the Obsidian Buttes swarm. Models of earthquake triggering by aseismic creep can explain both the time history of seismic activity associated with the 2005 swarm and the ~1 km/h migration velocity exhibited by this and several other Salton Trough earthquake swarms. A combination of earthquake triggering models and denser geodetic data should enable significant improvements in time-dependent forecasts of seismic hazard in the key days to hours before significant earthquakes in the Salton Trough.

Citation: Lohman, R. B., and J. J. McGuire (2007), Earthquake swarms driven by aseismic creep in the Salton Trough, California, *J. Geophys. Res.*, *112*, B04405, doi:10.1029/2006JB004596.

1. Introduction

[2] Attempts to understand the physical mechanisms controlling the timing of earthquake occurrence often focus on linking observations of changes in earthquake productivity to events that alter the stress state within the crust [*Dieterich*, 1994]. Common examples include the aftershock sequences triggered by large crustal earthquakes [e.g., *Freed and Lin*, 2001; *Helmstetter et al.*, 2006], seismic swarms [e.g., *Dieterich*, 1992; *Vidale and Shearer*, 2006; *Vidale et al.*, 2006], and long-term seismic cycles on major plate boundaries [e.g., *Dieterich*, 1994; *Lapusta et al.*, 2000]. The stressing rate changes associated with seismic swarms are often explained as a response to fault creep, fluid or magmatic events [e.g., *Hill et al.*, 1975; *Smith et al.*, 2004; *Hainzl and Ogata*, 2005; *McGuire et al.*, 2005; *Vidale and Shearer*, 2006; *Vidale et al.*, 2006], and have been exploited for evaluating earthquake triggering models in magmatically dominated environments [e.g., *Dieterich et al.*, 2000; *Toda et al.*, 2002]. *Davis et al.* [2001, 2004] use borehole pressure transients to infer that aseismic spreading processes trigger earthquake swarms along the Juan de Fuca ridge, but no geodetic observations exist to verify this hypothesis. A recent survey of high-precision earthquake locations demonstrated that earthquake clusters are common occurrences in southern California. *Vidale and Shearer* [2006] identified a relationship between the spatial dimensions and seismic moment of swarms suggesting that aseismic driving processes are a general feature of swarms, but no complementary information about ground deformation was available to constrain this process.

[3] In the Imperial Valley/Salton Trough region, the North America-Pacific plate boundary transitions between the predominantly strike-slip San Andreas system to the north and the divergent boundary in the Gulf of California (Figure 1). Shortly after the installation of seismic networks, it was recognized that this region had a higher level of seismic swarm activity than the rest of California [e.g., *Richter*, 1958; *Brune and Allen*, 1967; *Hill et al.*, 1975; *Johnson and Hadley*, 1976; *Reichle and Reid*, 1977], possibly driven by magmatic intrusions within the Salton Trough's divergent tectonic setting [*Hill*, 1977]. The considerable evidence of aseismic deformation along faults in this region [e.g., *Allen et al.*, 1972; *Hudnut and Sieh*, 1989; *Hudnut et al.*, 1989; *Lyons and Sandwell*, 2003], suggests that the effect of high geothermal gradients on fault dynamics [*Ben-Zion and Lyakhovsky*, 2006] may also contribute to swarm initiation.

[4] During the 2-week period beginning on 29 August 2005, the Southern California Seismic Network (SCSN) recorded a seismicity rate increase approaching 3 orders of magnitude in the region south of the Obsidian Buttes, within the Brawley Seismic Zone near the southern termination of the San Andreas Fault (Figure 1). Surface breaks were observed in the field in the days following the swarm (K. Hudnut, personal communication, 2005). We examine the available seismic and geodetic data associated with the Obsidian Buttes seismic swarm and determine that shallow aseismic slip is required during the swarm. Our results suggest that shallow aseismic fault slip was the primary

[1]Department of Earth and Atmospheric Sciences, Cornell University, Ithaca, New York, USA.
[2]Department of Geology and Geophysics, Woods Hole Oceanographic Institution, Woods Hole, Massachusetts, USA.

0148-0227/07/2006JB004596$09.00

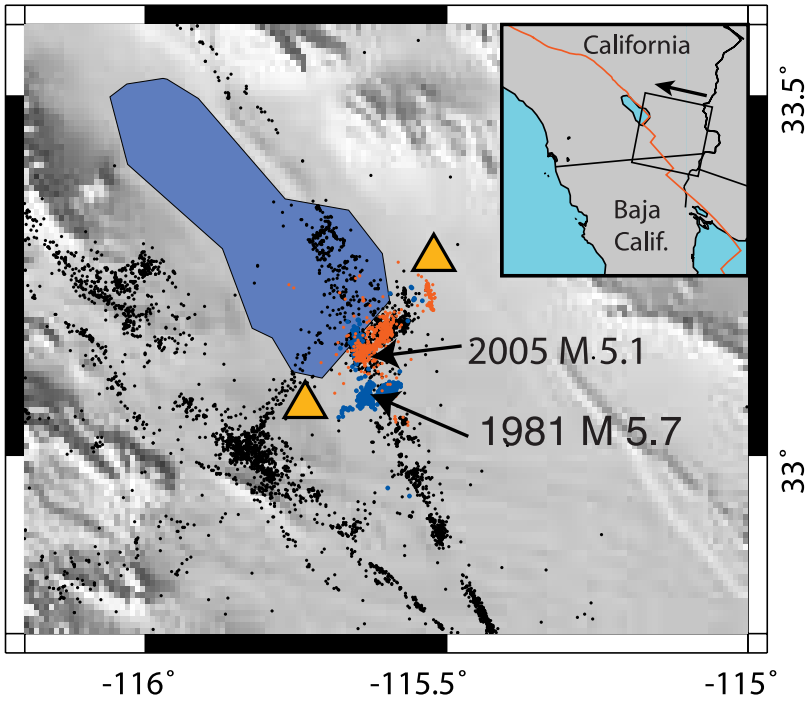

Figure 1. Map locating the 1981 and 2005 swarms. Yellow triangles indicate locations of GPS sites CRRS and GLRS. Blue and red dots show seismicity for the 1981 West Moreland and 2005 Obsidian Buttes earthquake swarms, respectively (see Figure 2 for detail of each swarm). Relocated seismicity [*Hauksson et al.*, 2003] from 1984 to 2002 is shown with black dots, and shaded relief is from http://www.ngdc.noaa.gov. Inset is a location map. Black rectangle indicates the InSAR data used in this study, from Envisat track 84, frame 2943, with arrow indicating line-of-sight (LOS) direction of InSAR satellite. Red line indicates the North America–Pacific plate boundary.

driving process behind this and other Salton Trough swarms.

2. Data and Modeling

[5] The Obsidian Buttes swarm is unique in that both well-recorded seismicity and geodetic observations exist spanning the sequence. Here we examine both types of data and compare the resulting predictions to identify the dominant processes occurring during the swarm.

2.1. Seismicity

[6] The abundant seismic data for the swarms in the Salton Trough provide an opportunity to image the space-time evolution of the seismicity during earthquake swarms. However, the standard (single event) catalog locations available from the Southern California Earthquake Data Center (SCEDC) lack the resolution to explore the details of swarm migration. We relocated both the Obsidian Buttes swarm and the 1981 West Moreland swarm, which occurred in the same area (Figure 1), using the double-difference algorithm of *Waldhauser and Ellsworth* [2000] (see the auxiliary material).[1] We relocated each swarm independently to minimize the effects of varying station configurations [*Rubin*, 2002]. Differential P and S traveltimes were calculated from the SCEDC phase picks. In addition, for the 2005 swarm, we also measured differential times directly from the archived waveform data for the $M < 3$ events (which were not clipped) using a frequency domain algorithm [*Schaff et al.*, 2002]. We only used arrival times with cross-correlation coefficients >0.8 in the inversion, resulting in approximately 47,000 waveform-derived and 500,000 catalog differential traveltimes for the 2005 swarm. We gave P wave measurements twice the weight of S wave measurements. Average residuals were on the order of 10 ms for waveform-derived times (2005 swarm) and 50 ms for catalog-derived arrival times (both swarms). The relocations utilized a 20-layer, one-dimensional (1-D) velocity model derived from the SCEC 3-D model version 4 at the location of the swarm [*Kohler et al.*, 2003].

[7] For the 1981 West Moreland swarm, the seismicity during the 130 hours preceding the largest (M_w 5.9) earthquake shows a complicated migration over a series of faults (Figures 2a and 3a). The main shock and its aftershocks occurred on a 10–15 km, NE striking fault segment just south of the seismicity in the first part of the swarm. Additionally, some events from the later part of the 1981 swarm occurred about 10 km north of the 1981 main shock on a N-S striking fault that is adjacent to the area that ruptured during the 2005 swarm. Bilateral migration of seismicity during the initial 100 hours of the 1981 swarm occurred at about 0.1 km/h.

[1] Auxiliary materials are available at ftp://ftp.agu.org/apend/jb/2006jb004596.

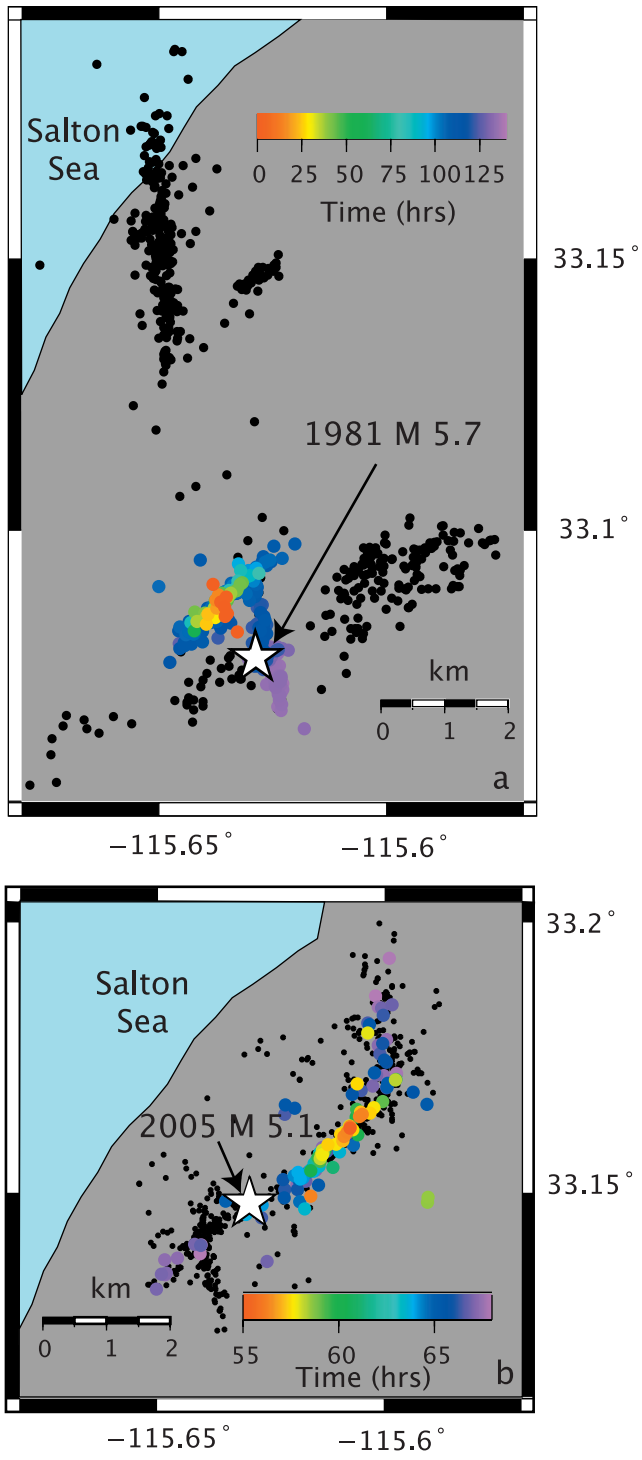

Figure 2. Spatiotemporal evolution of both swarms. Black dots show seismicity for (a) 1981 West Moreland and (b) 2005 Obsidian Buttes earthquake swarms, with the first few hours of seismicity colored by time since initiation of the swarm in each case (see Figure 3). The 1981 swarm propagated to the north in its later hours. Stars indicate the largest earthquake in each swarm.

[8] Relocations of the $M1-3$ events in the 2005 sequence (Figure 2b) indicate that seismic faulting was restricted to a narrow depth range (4–6 km) along a 10 km NE striking near-vertical fault segment. After 31 August (50 hours in Figures 2b and 3b) the seismic swarm exhibited a clear bilateral migration at roughly 0.5 km/h over the next 15 hours, somewhat faster than migration during the 1981 swarm. The time period of the migrating seismicity coincided with the highest seismicity rates during the swarm, but the largest earthquake, a strike-slip $M5.1$, did not occur until 2 September (star, Figure 3b).

[9] The orientation of the primary fault plane in the 2005 swarm is confirmed by the automated moment tensor waveform inversions done by the SCEDC (see Figure 4). Fifteen of the 17 events (M_w 3.3 to 5.1) with good variance reductions (>50%) have strike-slip mechanisms with a NE striking nodal plane coincident with the strike of the swarm as a whole. A few of the events near the ends of the fault segment may have occurred on more northerly conjugate planes (Figure 4).

2.2. Geodetic Data

[10] Surface deformation during the Obsidian Buttes swarm was observed by two nearby GPS stations within the Southern California Integrated GPS Network (SGIGN) and by interferometric synthetic aperture radar (InSAR).

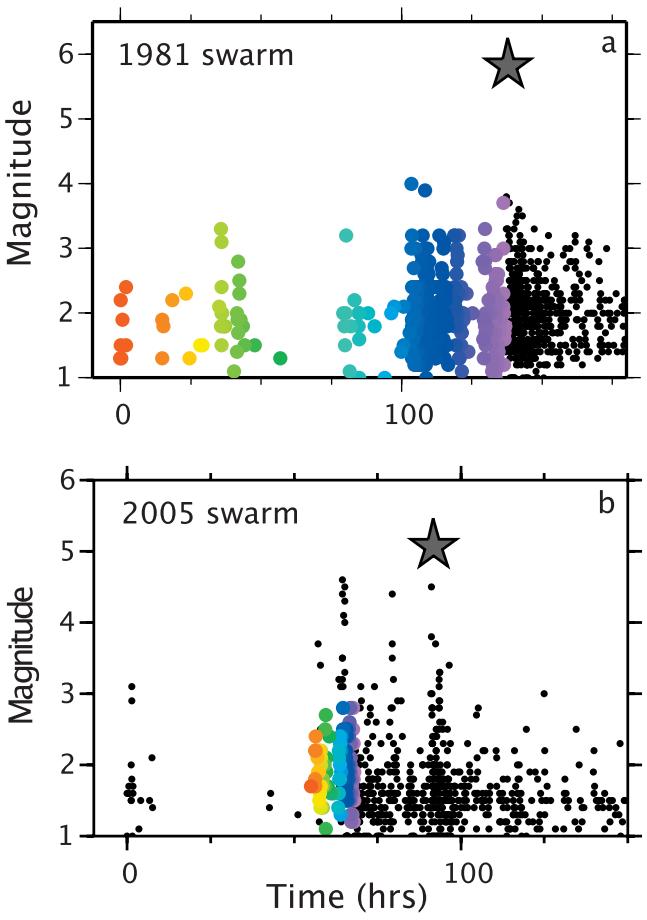

Figure 3. Earthquake magnitude versus time for the (a) 1981 and (b) 2005 swarms, with $M < 4$ colored by time as in Figure 2, and stars indicating the largest events.

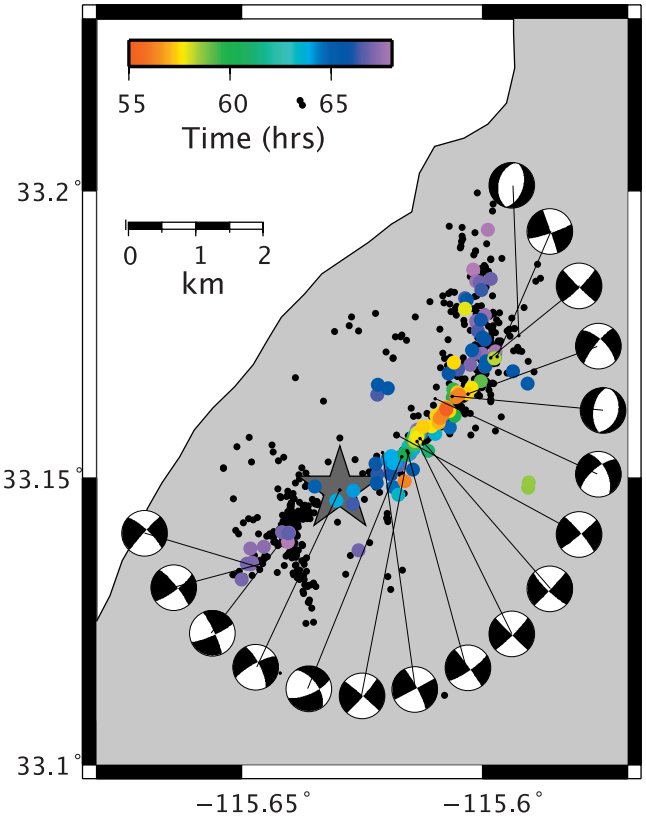

Figure 4. Focal mechanisms for the Obsidian Buttes swarm from the SCSN catalog. Colors and symbols are same as for Figure 2.

The GPS stations GLRS and CRRS are located 17 and 13 km away from the largest event within the swarm, respectively (Figure 1). An offset of ~5 mm in the north component of the GLRS-CRRS line length change evolved over the course of several days (Figure 5). Although the large distance between the GPS sites and the earthquakes results in a low signal-to-noise ratio, the data are consistent with the largest earthquake (red dashed line, Figure 5) occurring several days after the initiation of deformation.

[11] The Envisat satellite acquired InSAR data before and after the swarm, allowing formation of an interferogram constraining deformation that occurred during a 35-day period spanning the event, from 21 August 2005 to 25 September 2005 (track 84, frame 2943). We processed the InSAR data using the Jet Propulsion Laboratory California Institute of Technology ROI_PAC processing suite [*Rosen et al.*, 2004], removing the topographic signature from the interferometric phase with the 30-m Shuttle Radar Topography Mission (SRTM) digital elevation model (DEM) [*Farr and Kobrick*, 2000]. A clear signal is present in the vicinity of the swarm (Figures 6 and 7a) with a spatial extent of several tens of kilometers and a peak-to-peak magnitude of 14 cm in the satellite line-of-sight (LOS) direction, despite extensive decorrelation due to the presence of bodies of water, agricultural activity and sand dune drift (see the auxiliary material).

[12] The high rates of geothermal energy production in the area immediately around the Obsidian Buttes swarm require that we test whether the signal observed in Figure 6 could be anthropogenic. We examined interferograms for several other independent 35-day time intervals before and

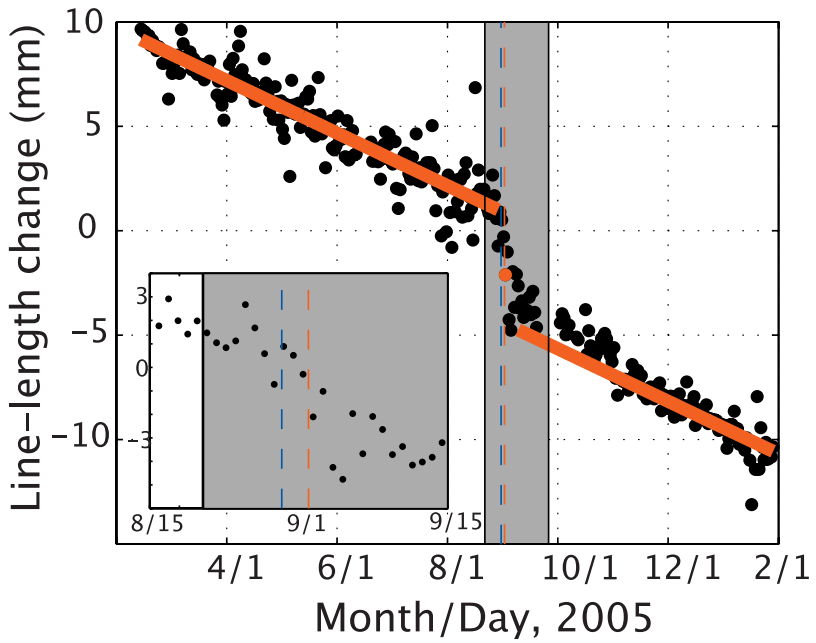

Figure 5. North component of line length change between SCIGN GPS stations CRRS and GLRS for 1-year and 1-month (inset) intervals spanning the 2005 swarm, with 24-hour Scripps Orbit and Permanent Array Center (SOPAC, http://sopac.ucsd.edu) solutions (black dots, red dot on day of largest earthquake), linear trends derived from fitting until a week before and 2 months after the swarm (heavy red lines), and time period of the interferogram (gray box). Dashed lines indicate swarm initiation (blue) and the *M*5.1 earthquake (red).

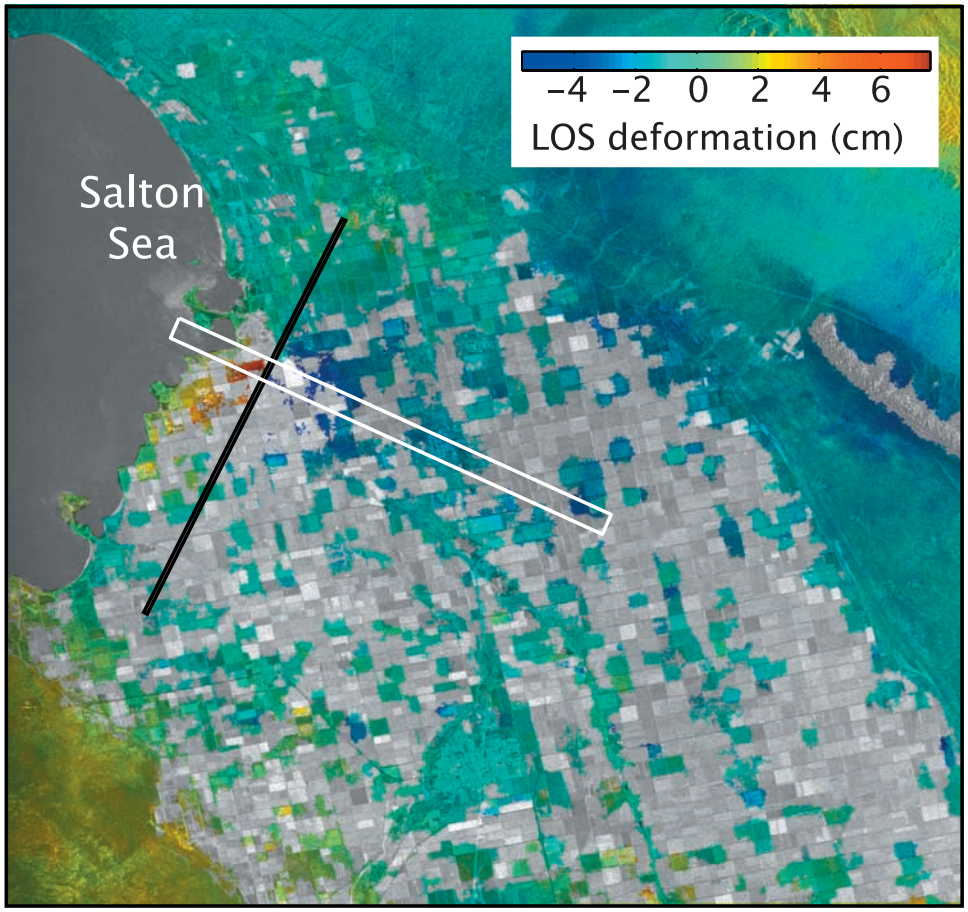

Figure 6. Interferogram phase (color) and amplitude (intensity) spanning 21 August 2005 to 25 September 2005. Gray regions indicate poor interferogram coherence. Rectangles indicate profile (white) and fault plane (black) used in Figure 7. Signals in upper right of image are likely due to atmospheric water vapor variations that vary over these longer spatial length scales.

after the earthquake and found no detectable signal in the region immediately around the deformation field associated with the Obsidian Buttes swarm (Figure 8).

2.3. Modeling

[13] We compared the geodetic observations with the deformation expected from the recorded seismicity alone to determine whether the observed displacement field requires a contribution from aseismic processes. We generated forward models of the ground deformation expected from the observed seismicity (1178 events) using finite dislocations in a linear elastic half-space [*Okada*, 1985] with rigidity modulus of 2.4×10^{10} Pa. The predicted deformation signal from seismicity alone is dominated by the three to four largest events. We calculated the magnitude of slip and fault patch size for each earthquake from the seismic moment assuming a 100-bar stress drop. We used reported mechanisms from the SCSN catalog (Figure 4) when available, and used the strike, dip and rake for the main earthquake for those smaller events with no reported mechanism. We note that these smaller earthquakes contribute a very small amount to the total deformation field. The combined recorded seismicity, which was equivalent to a M_w 5.3 earthquake and predicts peak LOS deformation of ~2 cm, is of insufficient magnitude to reproduce the InSAR signal spanning the swarm (Figure 7). Shifting the seismicity to shallower depths results in a closer match to the peak amplitude of ground deformation, but a shorter wavelength signal that does not fit the observed deformation (Figure 9).

[14] In order to better explain the geodetic data, we performed inversions of the InSAR data using a distribution of finite dislocations in the same elastic model as above, with a steeply dipping fault plane that agrees with the location and mechanisms of seismicity during the swarm (strike = N35°E, dip = 72°), and with fault patch sizes that increase with depth. We regularized the inversion using a minimum length constraint and allowed a combination of left-lateral and dip-slip motion [e.g., *Du et al.*, 1992; R. Lohman and M. Simons, Inferring fault slip from surface deformation using a spatially variable regularization scheme, submitted to *Geophysical Journal International*, 2006]. Our best fit slip distribution (Figure 7e) is dominated by dextral motion with slip equivalent to a M_w 5.75 earthquake (using the same rigidity structure that we used with the seismic data). Our results suggest a significant contribution to the observed ground deformation from aseismic slip, since the magnitude of slip we infer is five times larger than the seismic moment release observed

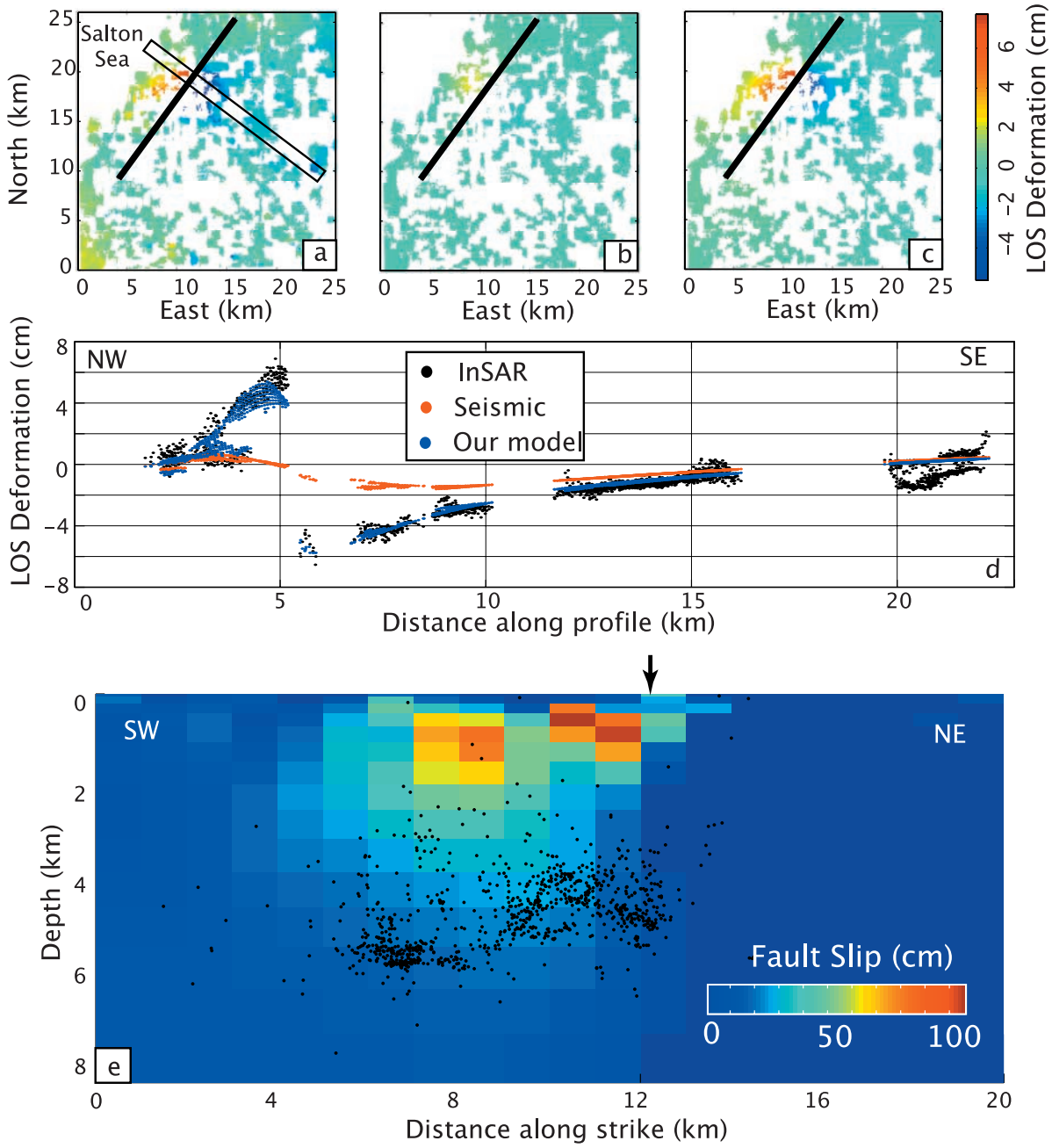

Figure 7. (a) Interferogram phase from Figure 6. Symbols are same as in Figure 6. (b–c) Forward models from observed seismicity and best-fit fault slip model, using same color scale as Figure 7a. (d) Cross-fault profile through Figures 7a–7c. (e) Best fit fault slip model (M_w 5.75), seismicity (black dots), and location of profile from Figure 7d (black arrow). Slip is primarily left-lateral.

during the Obsidian Buttes sequence. The majority of our inferred fault slip occurred at shallower depths than the seismicity, suggesting that different processes may accommodate the fault slip budget within these two depth ranges.

3. Discussion

3.1. Earthquake Triggering

[15] To investigate the hypothesis that shallow aseismic slip triggered the earthquake swarm, we employ the rate state formalism of *Dieterich* [1994], which relates changes in fault stress state to changes in seismicity rate. The time history of aseismic slip for this event is poorly resolved by the available geodetic data, but other shallow creep events in well-instrumented regions are observed to start abruptly and decay exponentially [e.g., *Nason and Weertman*, 1973; *Linde et al.*, 1996]. Therefore we model the creep event as an increase in stressing rate beginning at the start of the swarm migration, during the highest seismicity rates (Figure 10), and decaying exponentially over a timescale of a few

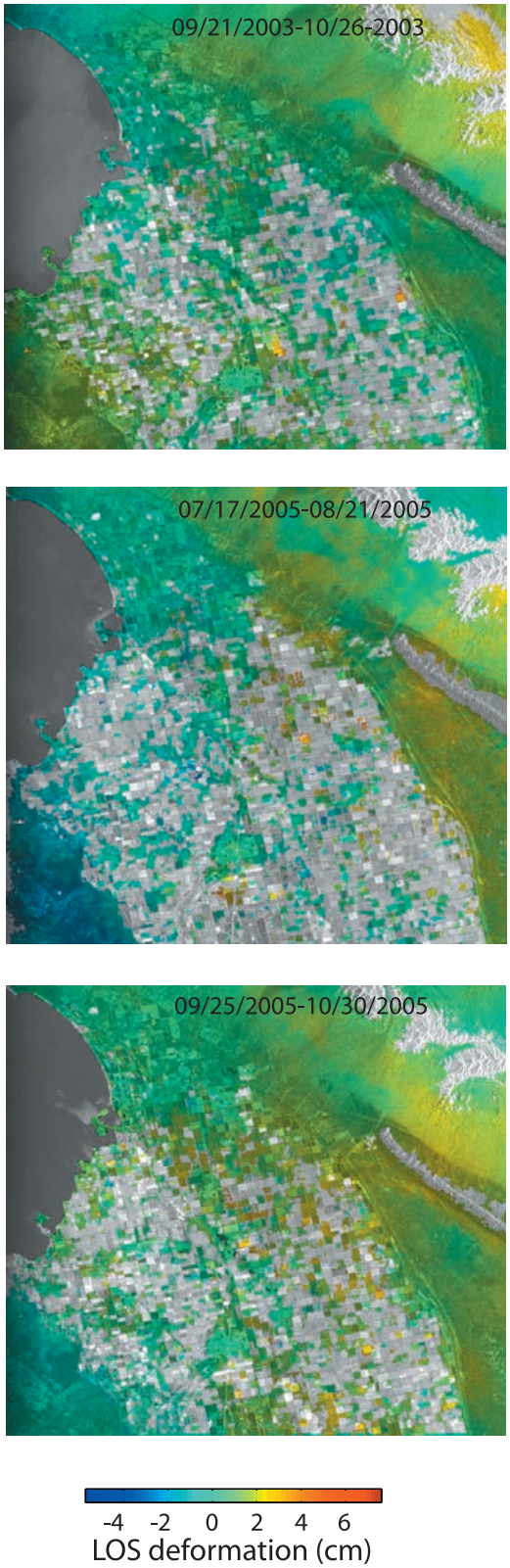

Figure 8. Phase (color) and amplitude (intensity) for typical interferograms in the Imperial Valley, spanning three different time intervals during the same time of year as the Obsidian Buttes swarm. Color scale is the same as in Figure 6.

days in a manner consistent with the GPS observations (Figure 5).

[16] We chose the background stressing rate (2 bars/yr) to correspond roughly to the 15 year recurrence interval of *M*5 earthquakes on this fault [*Reasenberg and Jones*, 1994], and we chose the stressing rate jump (factor of ~900) to match the observed peak seismicity rates. We explored a range of potential values of the rate state friction parameter $A\sigma$, which relates changes in stressing rate to seismicity rate [*Dieterich*, 1994], where A is a constitutive parameter and σ is the normal stress. Uncertainties in rock type and thermal state of the seismogenic zone complicate the determination of which values of $A\sigma$ are realistic. Nearby geothermal wells indicate that temperatures reach ~350°C by ~2 km depth [*Hulen and Pulka*, 2001]. The presence of aseismic slip in the 2–4 km depth range within sandstone sediments at these temperatures is consistent with laboratory experiments on frictional stability [*Blanpied et al.*, 1991]. We have little information on the deeper thermal structure in the depth range of the observed seismicity (4–6 km), but extrapolation of the thermal gradient from *Hulen and Pulka* [2001] leads to estimates as high as 460–590°C, well out of the range where frictional instability and earthquakes should occur in granitic materials [*Blanpied et al.*, 1991]. Hydrothermal circulation could significantly reduce the temperature gradient or the thermal structure in this area could vary over a shorter length scale than is sampled by the well data.

[17] The stressing rate magnitude primarily determines the maximum amplitude of the seismicity rate transient while the value of $A\sigma$ controls the decay timing (Figure 10). The seismicity rate history indicates that the majority of the aseismic stressing occurred between 31 August and 2 September, although a reduced level of aseismic slip for at least a few days after 2 September is required to match the

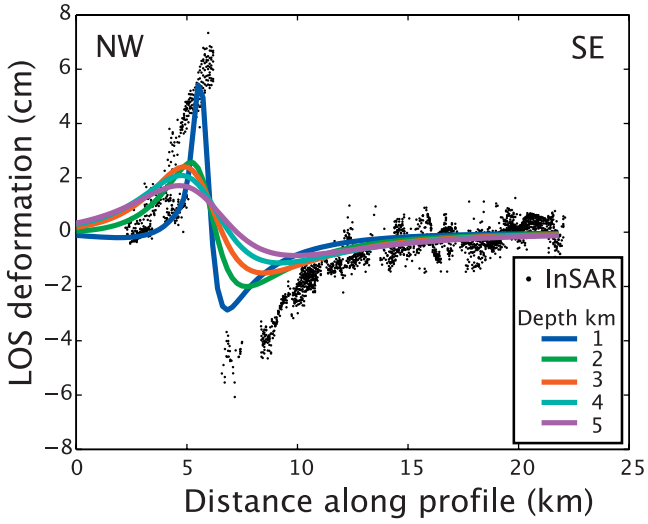

Figure 9. Data (black dots) from interferogram profile in Figure 7d and forward models of the ground deformation expected from observed seismicity, where the average depth of the swarm as a whole is shifted to depths between 1 and 5 km (colored lines). Note that even the shallowest depth range (blue line) does not match the peak magnitude or shape of the deformation.

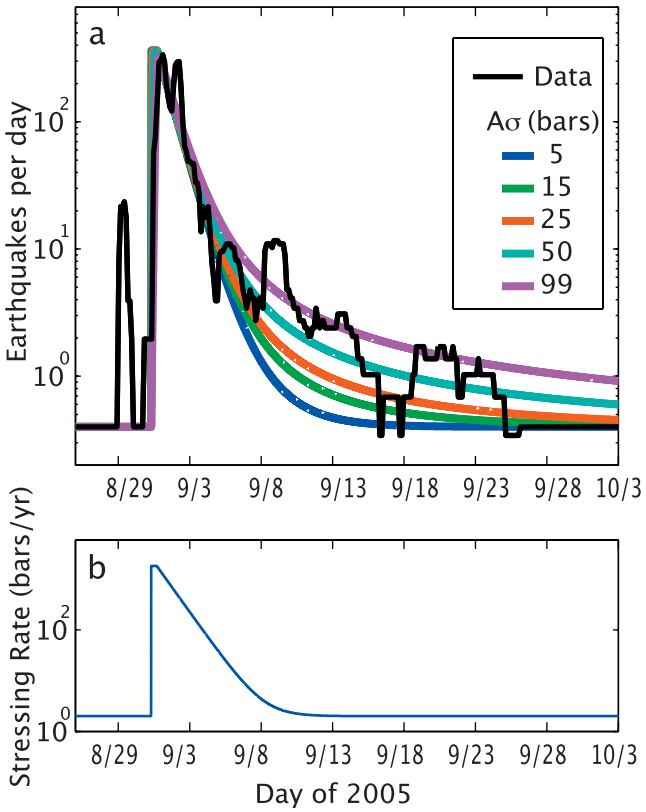

Figure 10. (a) Seismicity rate ($M > 1.5$) in the area immediately surrounding the 2005 Obsidian Buttes swarm (black curve), and predicted rates (colored curves) obtained by neglecting normal stress changes [*Dieterich*, 1994] for various values of the rate state friction parameter $A\sigma$. (b) Stressing rate history with exponential decay used in Figure 10a.

observed decay in seismicity. The elevated seismicity rate in the later days of the swarm (from 8 to 28 September) relative to the $A\sigma = 15$ bars curve in Figure 10a could indicate that the stressing rate history is more complicated than our exponential decay model.

[18] The correspondence between the observed seismicity and the prediction from our aseismic stressing rate history suggests that the migration and temporal evolution of the seismicity for this particular swarm could have been driven by aseismic slip occurring in the early hours of the swarm, well before the largest earthquake. Studies of future swarms may be able to rely on denser geodetic observations that place stronger constraints on the temporal evolution of strain, allowing for more meaningful evaluations of the range of rate state friction parameters that are appropriate.

3.2. Other Seismic Swarms

[19] Other swarms within the Salton Trough exhibit similar features to those we observed during the Obsidian Buttes swarm, indicating that a common mechanism may drive the swarms. Migration velocities for several Salton Trough swarms (Table 1) are in the range of 0.1–1 km/h, similar to the 0.1–0.5 km/h that we observe for the West Moreland and Obsidian Buttes swarms. *Brune and Allen* [1967] describe a 10 km long surface rupture with offsets of only ~1.5 cm that was detected following a sequence of small earthquakes ($M < 3.6$) on 4 March 1966. While *Brune and Allen* [1967] argue that the 1966 event could have been a seismic rupture with an extremely low stress drop, Figure 1 of Brune and Allen demonstrates the northward propagation of the sequence at a velocity of ~1 km/h. The similarity in propagation rate suggests to us that the 1966 swarm may also have been associated with shallow aseismic slip. Another swarm on the Imperial fault in 1975 [*Johnson and Hadley*, 1976] migrated at 0.5 km/h over a similar length scale. Additionally, creep events along the Cerro Prieto fault, the primary plate boundary in northern Baja California, propagate at about 1 km/h [*Glowacka et al.*, 2001].

[20] The 0.1–1 km/h migration velocity that appears to be typical of strike-slip swarms in the Salton Trough contrasts with observations of swarms associated with fluid diffusion within fault zones that migrate at much slower rates of fractions of a kilometer per day [*Hainzl and Ogata*, 2005] but agrees with well-documented creep events along the central San Andreas Fault [e.g., *Nason and Weertman*, 1973; *Linde et al.*, 1996]. The systematic migration velocities and their similarity to geodetically observed creep events support the hypothesis that earthquake swarms in the Salton Trough are triggered by transient, aseismic, fault slip.

[21] Aseismic triggering as an explanation for seismic swarms extends to other regions around the world as well. East Pacific Rise transform faults, which potentially share the same high heat flow characteristics found in the Salton Trough, exhibit heightened levels of seismicity preceding large strike-slip earthquakes [e.g., *McGuire et al.*, 2005; *Bohnenstiehl et al.*, 2002] that is reminiscent of the microseismicity increases in the hours before the Salton Trough earthquakes. *Vidale and Shearer* [2006] and *Vidale et al.* [2006] find that aseismic processes may drive earthquake swarms throughout southern California and in Japan. The 0.1–1 km/h migration velocities observed in Salton Trough swarms also appear to be characteristic of slow slip events in subduction zones both in Cascadia [e.g., *Dragert et al.*, 2001; *McGuire and Segal*, 2003] and Japan [e.g., *Obara*, 2002; *Shelly et al.*, 2006; Y. Ishihara, personal communication, 2006]. To advance our understanding of the contribution from aseismic processes to plate boundary deformation around the world, we require combined geodetic and seismicity observations of the sort outlined here,

Table 1. Moderate to Large Earthquakes in the Salton Trough/Imperial Valley Region With Documented Preearthquake Sequences Characterized as Either Foreshock Activity or Seismic Swarms

Date	Magnitude	Fault	Sequence Length, hours
1955	*M*5.3	Brawley [*Richter*, 1958]	30
1955	*M*5.4	Brawley [*Richter*, 1958]	2
1976	*M*5.7	Cerro Prieto [*Gonzalez et al.*, 1984]	100
1980	M_w6.3	Cerro Prieto [*Wong et al.*, 1997]	20
1981	M_w5.9	West Moreland(this study)	100
1987	M_w6.0–6.5	Elmore Ranch/Superstition Hills [*Magistrale et al.*, 1989]	1
2005	M_w5.1	Obsidian Buttes (this study)	50

along with improved constraints on the temporal evolution of ground deformation.

4. Conclusions

[22] The geodetic data for the 2005 Obsidian Buttes swarm present the first evidence that detectable levels of aseismic slip may trigger moderate earthquakes in the Salton Trough. The observed consistency in seismicity migration velocities for the 1966, 1975, 1981, and 2005 Salton Trough swarms indicates the existence of a common driving mechanism. Currently, real-time earthquake forecasts are based solely on stochastic models of past seismicity without input from other geophysical data types or mechanical models of earthquake triggering [e.g., *Gerstenberger et al.*, 2005; *Helmstetter et al.*, 2006]. A combination of dense real-time geodetic networks, algorithms that search for propagating microseismicity, and mechanical triggering models, should significantly improve short-term earthquake forecasts within the Salton Trough.

[23] **Acknowledgments.** We are grateful to K. Hudnut, M. Rymer, and K. Kendrick for helpful discussions and comments and to J. Vidale and R. Burgmann for their detailed and constructive reviews. Envisat SAR imagery was acquired from Eurimage, Italy, under a category 1 research proposal. GMT mapping software [*Wessel and Smith*, 1998] was used to prepare figures. This material is based upon work supported by the National Science Foundation under grant 0548785. R.B.L. was supported by a WHOI postdoctoral research fellowship.

References

Allen, C. R., M. Wyss, J. N. Brune, A. Grantz, and R. E. Wallace (1972), Displacements on the Imperial, Superstition Hills, and San Andreas faults triggered by the Borrego Mountain earthquake, *U.S. Geol. Surv. Prof. Pap.*, *787*, 87–104.

Ben-Zion, Y., and V. Lyakhovsky (2006), Analysis of aftershocks in a lithospheric model with seismogenic zone governed by damage rheology, *Geophys. J. Int.*, *165*, 197–210.

Blanpied, M. L., D. A. Lockner, and J. D. Byerlee (1991), Fault stability inferred from granite sliding experiments at hydrothermal conditions, *Geophys. Res. Lett.*, *18*, 609–612.

Bohnenstiehl, D. R., M. Tolstoy, R. P. Dziak, C. G. Fox, and D. K. Smith (2002), Aftershock sequences in the mid-ocean ridge environment: An analysis using hydroacoustic data, *Tectonophysics*, *354*, 49–70.

Brune, J. N., and C. R. Allen (1967), A low-stress-drop, low-magnitude earthquake with surface faulting: The Imperial, California earthquake of March 4, 1966, *Bull. Seismol. Soc. Am.*, *57*, 501–514.

Davis, E., K. Wang, R. E. Thompson, K. Becker, and J. F. Cassidy (2001), An episode of seafloor spreading and associated plate deformation inferred from crustal fluid pressure transients, *J. Geophys. Res.*, *106*, 21,953–21,963.

Davis, E., K. Becker, R. Dziak, J. Cassidy, K. Wang, and M. Lilley (2004), Hydrological response to a seafloor spreading episode on the Juan de Fuca ridge, *Nature*, *430*, 335–338.

Dieterich, J. (1994), A constitutive law for rate of earthquake production and its application to earthquake clustering, *J. Geophys. Res.*, *99*, 2601–2618.

Dieterich, J., V. Cayol, and P. Okubo (2000), The use of earthquake rate changes as a stress meter at Kilauea Volcano, *Nature*, *408*, 457–460.

Dieterich, J. H. (1992), Earthquake nucleation on faults with rate- and state-dependent friction, *Tectonophysics*, *211*, 115–134.

Dragert, H., K. Wang, and T. S. James (2001), A silent slip event on the deeper Cascadia subduction interface, *Science*, *292*, 1525–1528.

Du, Y., A. Aydin, and P. Segall (1992), Comparison of various inversion techniques as applied to the determination of a geophysical deformation model for the 1983 Borah Peak earthquake, *Bull. Seismol. Soc. Am.*, *82*, 1840–1866.

Farr, T. G., and M. Kobrick (2000), Shuttle radar topography mission produces a wealth of data, *Eos Trans. AGU*, *81*, 583.

Freed, A. M., and J. Lin (2001), Delayed triggering of the 1999 Hector Mine earthquake by viscoelastic stress transfer, *Nature*, *411*, 180–183.

Gerstenberger, M. C., S. Wiemer, L. M. Jones, and P. A. Reasenberg (2005), Real-time forecasts of tomorrow's earthquakes in California, *Nature*, *435*, 328–331.

Glowacka, E., J. J. Gonzalez, F. A. Nava, F. Farfan, and G. Diaz de Cossio (2001), Monitoring surface deformation in the Mexicali Valley, B. C., Mexico, paper presented at the 10th FIG International Symposium on Deformation Measurements, Calif. Inst. of Technol., Orange, Calif.

Gonzalez, J. J., F. A. Nava, and C. A. Reyes (1984), Foreshock and aftershock activity of the 1976 Mesa de Andrade, Mexico earthquake, *Bull. Seismol. Soc. Am.*, *74*, 223–233.

Hainzl, S., and Y. Ogata (2005), Detecting fluid signals in seismicity data through statistical earthquake modeling, *J. Geophys. Res.*, *110*, B05S07, doi:10.1029/2004JB003247.

Hauksson, E., W.-C. Chi, P. Shearer, and A. Michael (2003), Comprehensive waveform cross-correlation of southern California seismograms: part 1. Refined hypocenters obtained using the double-difference method and tectonic implications, *Eos Trans. AGU*, *84*(46), Fall Meet. Suppl., Abstract S21D-0326.

Helmstetter, A., Y. Y. Kagan, and D. D. Jackson (2006), Comparison of short-term and time-independent earthquake forecast models for Southern California, *Bull. Seismol. Soc. Am.*, *96*, 90–106.

Hill, D. P. (1977), A model for earthquake swarms, *J. Geophys. Res.*, *82*, 1347–1352.

Hill, D. P., P. Mowinckel, and L. G. Peake (1975), Earthquakes, active faults, and geothermal areas in the Imperial Valley, California, *Science*, *188*, 1306–1308.

Hudnut, K., and K. E. Sieh (1989), Behavior of the Superstition Hills fault during the past 330 years, *Bull. Seismol. Soc. Am.*, *79*, 304–329.

Hudnut, K. W., L. Seeber, and J. Pacheco (1989), Cross-fault triggering in the November 1987 Superstition Hills earthquake sequence, southern California, *Geophys. Res. Lett.*, *16*, 199–202.

Hulen, J. B., and F. S. Pulka (2001), Newly-discovered, ancient extrusive rhyolite in the Salton Sea Geothermal Field, Imperial Valley, California, paper presented at Twenty-Sixth Workshop on Geothermal Reservoir Engineering, Stanford Univ., Stanford, Calif.

Johnson, C. E., and D. M. Hadley (1976), Tectonic implications of the Brawley earthquake swarm, Imperial Valley, California, January 1975, *Bull. Seismol. Soc. Am.*, *66*, 1133–1144.

Kohler, M., H. Magistrale, and R. Clayton (2003), Mantle heterogeneities and the SCEC three-dimensional seismic velocity model version 3, *Bull. Seismol. Soc. Am.*, *93*, 757–774.

Lapusta, N., J. R. Rice, Y. Ben-Zion, and G. Zheng (2000), Elastodynamic analysis for slow tectonic loading with spontaneous rupture episodes on faults with rate- and state-dependent friction, *J. Geophys. Res.*, *105*, 23,765–23,789.

Linde, A. T., M. T. Gladwin, M. J. S. Johnston, R. L. Gwyther, and R. G. Bilham (1996), A slow earthquake sequence on the San Andreas fault, *Nature*, *383*, 65–68.

Lyons, S., and D. Sandwell (2003), Fault creep along the southern San Andreas from interferometric synthetic aperture radar, permanent scatterers, and stacking, *J. Geophys. Res.*, *108*(B1), 2047, doi:10.1029/2002JB001831.

Magistrale, H. W., et al. (1989), The Superstition Hills, California, earthquakes of 24 November 1987, *Bull. Seismol. Soc. Am.*, *79*, 239–251.

McGuire, J. J., and P. Segal (2003), Imaging of aseismic fault slip transients recorded by dense geodetic networks, *Geophys. J. Int.*, *155*, 778–788.

McGuire, J. J., M. Boettcher, and T. H. Jordan (2005), Foreshock sequences and short-term earthquake predictability on East Pacific Rise transform faults, *Nature*, *434*, 457–461.

Nason, R. D., and J. Weertman (1973), A dislocation theory analysis of fault creep events, *J. Geophys. Res.*, *78*, 7745–7751.

Obara, K. (2002), Nonvolcanic deep tremor associated with subduction in southwest Japan, *Science*, *296*, 1679–1681.

Okada, Y. (1985), Surface deformation due to shear and tensile faults in a half-space, *Bull. Seismol. Soc. Am.*, *75*, 1135–1154.

Reasenberg, P. A., and L. M. Jones (1994), Earthquake aftershocks: Update, *Science*, *265*, 1251–1252.

Reichle, M., and I. Reid (1977), Detailed study of earthquake swarms from the Gulf of California, *Bull. Seismol. Soc. Am.*, *87*, 159–171.

Richter, C. F. (1958), *Elementary Seismology*, W. H. Freeman, New York.

Rosen, P. A., S. Hensley, G. Peltzer, and M. Simons (2004), Updated repeat orbit interferometry package released, *Eos Trans. AGU*, *85*, 47.

Rubin, A. M. (2002), Using repeating earthquakes to correct high-precision earthquake catalogs for time-dependent station delays, *Bul. Seismol. Soc. Am.*, *92*, 1647–1659.

Schaff, D. P., G. H. R. Bokelmann, G. C. Beroza, F. Waldhauser, and W. L. Ellsworth (2002), High-resolution image of Calaveras Fault seismicity, *J. Geophys. Res.*, *107*(B9), 2186, doi:10.1029/2001JB000633.

Shelly, D. R., G. C. Beroza, S. Ide, and S. Nakamula (2006), Low-frequency earthquakes in Shikoku, Japan, and their relationship to episodic tremor and slip, *Nature*, *442*, 188–191.

Smith, K. D., D. von Seggern, G. Blewitt, L. Preston, J. G. Anderson, B. Wernicke, and J. Davis (2004), Evidence for deep magma injection beneath Lake Tahoe, Nevada-California, *Science*, *305*, 1277–1280.

Toda, S., R. S. Stein, and T. Sagiya (2002), Evidence from the ad 2000 izu islands earthquake swarm that stressing rate governs seismicity, *Nature*, *419*, 58–61.

Vidale, J. E., and P. M. Shearer (2006), A survey of 71 earthquake bursts across southern California: Exploring the role of pore fluid pressure fluctuations and aseismic slip as drivers, *J. Geophys. Res.*, *111*, B05312, doi:10.1029/2005JB004034.

Vidale, J. E., K. L. Boyle, and P. M. Shearer (2006), Crustal earthquake bursts in California and Japan: Their patterns and relation to volcanoes, *Geophys. Res. Lett.*, *33*, L20313, doi:10.1029/2006GL027723.

Waldhauser, F., and W. L. Ellsworth (2000), A double-difference earthquake location algorithm: Method and application to the northern Hayward fault, California, *Bull. Seismol. Soc. Am.*, *90*(6), 1353–1368, doi:10.1785/0120000006.

Wessel, P., and W. H. F. Smith (1998), New, improved version of Generic Mapping Tools released, *Eos Trans. AGU*, *79*, 579.

Wong, V., J. Frez, and F. Suarez (1997), The Victoria, Mexico, earthquake of June 9, 1980, *Geofis. Int.*, *36*, 139–159.

R. B. Lohman, Department of Earth and Atmospheric Sciences, Cornell University, Ithaca, NY 14850, USA. (rolohman@gmail.com)

J. J. McGuire, Department of Geology and Geophysics, Woods Hole Oceanographic Institution, Woods Hole, MA 02543, USA. (jmcguire@whoi.edu)